Published in final edited form as:

ACS Chem Biol. 2022 December 16; 17(12): 3435–3449. doi:10.1021/acschembio.2c00574.

Yeast Display Enables Identification of Covalent Single Domain Antibodies Against Botulinum Neurotoxin Light Chain A

Rafael Alcala-Torano[1], **Mariha Islam**[1], **Jaclyn Cika**[2], **Kwok Ho Lam**[3], **Rongsheng Jin**[3], **Konstantin Ichtchenko**[2], **Charles B. Shoemaker**[4], **James A. Van Deventer**[1,5,*]

[1]Chemical and Biological Engineering Department, Tufts University, Medford, Massachusetts 02155, United States of America

[2]Department of Biochemistry and Molecular Pharmacology, New York University Grossman School of Medicine, New York, New York 10016, United States of America

[3]Department of Physiology and Biophysics, University of California, Irvine, California 92697, United States of America

[4]Tufts Cummings School of Veterinary Medicine, North Grafton, Massachusetts 01536, United States of America

[5]Biomedical Engineering Department, Tufts University, Medford, Massachusetts 02155, United States of America

Abstract

While covalent drug discovery is reemerging as an important route to small molecule therapeutic leads, strategies for the discovery and engineering of protein-based irreversible binding agents remain limited. Here, we describe the use of yeast display in combination with noncanonical amino acids (ncAAs) to identify irreversible variants of single-domain antibodies (sdAbs), also called VHHs and nanobodies, targeting botulinum neurotoxin light chain A (LC/A). Starting from a series of previously described, structurally characterized sdAbs, we evaluated the properties of antibodies substituted with reactive ncAAs capable of forming covalent bonds with nearby groups after UV irradiation (when using 4-azido-L-phenylalanine) or spontaneously (when using *O*-(2-bromoethyl)-L-tyrosine). Systematic evaluations in yeast display format of more than 40 ncAA-substituted variants revealed numerous clones that retain binding function while gaining either UV-mediated or spontaneous crosslinking capabilities. Solution-based analyses indicate that ncAA-substituted clones exhibit site-dependent target specificity and crosslinking capabilities

[*]**Corresponding author:** Dr. James A. Van Deventer, James.Van_Deventer@tufts.edu, P: (+1) (617) 627-6339.

5. Conflicts of Interest

R. A. -T., J. A. V. and C. B. S. are listed as inventors in a provisional patent application filed by Tufts University titled “Cross-linkable Single Domain Antibodies that Covalently Bind to a Target Antigen and Methods of Use Thereof.” K. I. is a founder and has financial interests in CytoDel Inc. During this study, K. I. consulted for CytoDel Inc. K. I. is inventor on patent US007785606B2, titled “Genetically engineered clostridial genes, proteins, encoded by the engineered genes, and uses thereof,” and US008980284B2, titled “Recombinant derivatives of botulinum neurotoxins engineered for trafficking studies and neuronal delivery.” K. I. is also inventor on patent application WO2016/094555A1 titled “Clostridial neurotoxin fusion proteins, propeptide fusions, their expression, and use.”

6. Supporting Information

The Supporting Information is available free of charge via the internet at http://pubs.acs.org. Materials and methods, DNA and protein sequences, and supporting figures including detailed flow cytometry data, SDS-PAGE, western blots, activity assays, mass spectrometry, and additional supporting figures (S1–S25).

uniquely conferred by ncAAs. Interestingly, not all ncAA substitution sites resulted in crosslinking events, and our data showed no apparent correlation between detected crosslinking levels and distances between sdAbs and LC/A residues. Our findings highlight the power of yeast display in combination with genetic code expansion in the discovery of binding agents that covalently engage their targets. This platform streamlines the discovery and characterization of antibodies with therapeutically relevant properties that cannot be accessed in the conventional genetic code.

2. Introduction

The establishment of antibodies as therapeutic agents has both promoted and benefited from modern biotechnology strategies that seek to improve antibody “drug-likeness” for pharmaceutical applications. Particularly, high-throughput display technologies have been used to engineer not only high potency and selectivity of antibodies and alternative binding scaffolds,[1–5] but also other desirable physicochemical characteristics such as stability,[6–8] solubility,[9] and even environmental responsiveness.[10, 11]

Although many properties can now be introduced or engineered into antibodies, the limited range of chemical functionalities in the genetic code still constrains the range of properties that are accessible. In particular, covalent target engagement is a property that is nearly impossible to access in antibodies. On the other hand, a growing number of small molecule drugs and drug leads possess chemical groups that facilitate the formation of covalent bonds with their respective biological targets. Covalent bond formation is useful for extended duration of action and sustained inhibition of target function and has even been shown to overcome acquired drug resistance.[12–15] The systematic introduction of these functionalities into proteins provides opportunities for leveraging the exquisite specificities of antibodies while accessing reactivities beyond what is enabled by the amino acids contained within the conventional genetic code.

Primary strategies for generating covalent protein adducts involve the use of either photocrosslinkable or spontaneously crosslinkable functional groups. Upon irradiation with light, photoreactive groups form reactive species that covalently engage with nearby residues and can convert a noncovalent interaction into a covalent one. Photocrosslinking has proven useful for in vitro investigations and protein profiling,[16–22] but its dependence on short-wavelength irradiation limits its use in therapeutics and other in vivo applications. Conversely, spontaneous crosslinking is mediated by proximity-enhanced reactivity to initiate covalent bond formation. This is an attractive strategy for therapeutics since it obviates the need for external stimuli to promote covalent target engagement.[23–28]

Two main approaches have been exploited to expand the chemical landscape of proteins with groups that can participate in covalent binding. The first one relies on the installation of chemical warheads by targeting designed cysteine residues,[29, 30] while the other is based on the incorporation of reactive noncanonical amino acids (ncAAs) via genetic code expansion, which can react with the intended target via several functional groups found within canonical amino acids.[23, 24, 26–28, 31] While each of these strategies has demonstrated the utility of engineering protein-based irreversible binding agents, they rely on solution-phase measurements to discover and validate crosslinking events. Thus, introducing such

reactivity into antibodies has yet to benefit from platforms capable of high throughput campaigns that can streamline discovery, engineering, and characterization processes prior to performing more detailed in-solution characterizations of promising leads.

Here we describe the use of yeast display, coupled with high resolution binding site structural information, to identify and characterize protease-inhibiting camelid single domain antibodies (sdAbs) capable of covalently binding to botulinum neurotoxin light chain A1 (LC/A) via reactive ncAAs. LC/A is a zinc-dependent protease responsible for the paralytic effects of botulism from exposure to Botulinum neurotoxins (BoNTs) and has become an attractive target of small molecule-based irreversible inhibition strategies[32–35] to address its long-lasting effects in the neuronal cytosol. Furthermore, recent reports demonstrate the ability to deliver sdAbs to intoxicated neurons to treat botulism in animals using an atoxic BoNT delivery vehicle.[36, 37]

In this work, we used two ncAAs, 4-azido-L-phenylalanine (AzF) and *O*-(2-bromoethyl)-L-tyrosine (OBeY) (Figure 1a), to introduce crosslinking functionality into sdAbs via light-mediated and spontaneous crosslinking, respectively.[16, 22–24, 27] Assays in yeast display format revealed numerous ncAA-substituted sdAb variants that retained binding function and led to the identification of photocrosslinkable and spontaneously crosslinkable variants exhibiting time-dependent crosslinking behaviors. Corroboration of key observations on the yeast surface with solution-phase experiments indicated that this display platform can be used to discriminate between reversible and irreversible covalent binding agents and to characterize their time-dependent behavior. Further experiments with purified sdAbs revealed that the reactive sdAbs retain their inhibitory properties against LC/A, and that ncAA substitution position can impact crosslinking selectivity in complex mixtures. Our findings not only underscore the utility of yeast display for the discovery of chemically augmented sdAbs, but also open up new opportunities to further engineer the selectivity and reactivity of these novel macromolecules using tools with high throughput capabilities.

3. Results and Discussion

3.1 Single-domain antibody mutant design and orthogonal translation system

To maximize the probability of identifying ncAA-substituted sdAbs that facilitate irreversible binding, we utilized a set of well-characterized, alpaca-derived sdAbs that target different epitopes of the light chain (LC) of botulinum neurotoxin serotype A1 (BoNT/A), and for which detailed structural binding data was available.[38, 39] We reasoned that targeting different regions of LC/A with ncAA-substituted sdAbs would increase the likelihood of identifying sites conducive to covalent bond formation (Figure 1). Based on the available crystallographic data of sdAb-LC/A complexes,[38, 39] we identified ncAA substitution sites in four sdAbs at positions likely to result in covalent interaction. Three of the chosen sdAbs, JPU-A5, JPU-C1, and JPU-C10, are potent inhibitors of LC/A protease activity (Figure 1b, c)[38] and one LC/A-binding sdAb, ciA-H7, has no protease inhibition activity but prevents BoNT/A intoxication of neuronal cells (Figure 1b, c).[39]

Guided by these sdAb-LC/A complex structures, we identified substitution positions in sdAbs that we deemed likely to result in photocrosslinking to LC/A based on 1) our recent

developments in studying AzF-mediated photocrosslinking events on the yeast surface;[22] and 2) access to the AcFRS orthogonal translation system (OTS) to introduce this ncAA in response to the TAG codon in *S. cerevisiae* (Figure 1b, c).[22, 40, 41]. Given the expected high reactivity of photoactivated AzF, the selected mutations were determined by the proximity between the chosen sdAb residue and the closest LC/A contacts, independently of the type of residue on the LC/A surface. In addition, we chose several positions (JPU-A5 Q1; JPU-C10 Q1, Q44 and Y111; ciA-H7 Q1) that lie further away from the sdAb-LC/A interface with future investigations of conjugation-mediated augmentation of sdAb properties in mind, but still evaluated the properties of the resulting clones in this work. In general, the mutations were localized to complementarity determining regions (CDRs). However, we also included several framework positions, particularly when substituting aromatic residues with the goal of minimizing structural disruptions but still presenting chemical functionality within proximity of the LC/A target.

Although our original intent was to identify positions amenable for photocrosslinked interactions, we recognized an opportunity to probe our mutant collection in the context of spontaneous crosslinking. Inspired by studies on the reactivity of electrophilic ncAAs,[23, 24] we utilized OBeY due to its structural similarity to other encodable ncAAs in yeast and its commercial availability. Given the known polyspecificity of AcFRS,[40] we evaluated the incorporation of OBeY with this synthetase by using a dual fluorescent reporter.[42] The results indicated that AcFRS supports moderately efficient OBeY incorporation in response to the TAG codon (Figure S1). With our designed mutants in hand and a suitable OTS to incorporate our chosen ncAAs, we proceeded to experimentally prepare these constructs in display format and evaluate their performance in binding to the target LC/A protease.

3.2 Display and binding validation

To streamline our investigations of ncAA-substituted sdAbs, we prepared all variants in yeast display format to evaluate binding and crosslinking properties. We cloned each wild type (WT) gene into the pCTCON2 vector[43] encoding for the sdAb antibody tethered to the C-terminus of the Aga2p protein. We chose this particular display orientation due to the important protein contacts that occur between LC/A and the CDR3 loops of the sdAbs, which are located near the C-termini of the sdAbs. It is possible that displaying sdAbs as N-terminal fusions to Aga2p would position CDR3 loops close enough to Aga2p to interfere with LC/A binding. During secretion, Aga2p gets covalently linked to the Aga1p protein and transferred to the yeast surface, resulting in display of the sdAb. The sdAb is flanked by HA and cMyc tags at the N and C terminus, respectively, allowing for detection of the full-length sdAb by labeling for the cMyc tag with fluorescently labeled reagents (Figure 1d). The mutant plasmids were constructed by introducing TAG codons at the selected positions using typical Gibson assembly procedures (see also Materials and Methods). *S. cerevisiae* RJY100[44] was transformed with the corresponding pCTCON2 plasmid and pRS315_KanRMod_AcFRS,[22, 40, 41] which encodes for the AcFRS tRNA aminoacyl synthetase and the corresponding orthogonal $tRNA_{CUA}$ for incorporation of ncAAs in response to the TAG codon.

We evaluated the display of the sdAbs and their ability to bind to LC/A after induction in the absence of ncAA or in the presence of 1 mM AzF or OBeY. After incubation of induced cells with LC/A and removal of excess protease the cells were treated with reagents to detect the C-terminal cMyc tag of the sdAb and the C-terminal Strep-tag of LC/A. Flow cytometry analysis showed a dependence of cMyc signal on the presence of ncAA during induction for the TAG mutants, but not for the WT constructs, confirming the expected behavior stemming from truncation due to the lack of ncAA (and thus lack of stop codon suppression; Figures 2a, b, S2–S4). We detected binding to LC/A for nearly all variants containing AzF or OBeY, while no LC/A binding was observed in samples induced in the absence of ncAAs. LC/A was not detected in any of our non-binding protein controls, either (scFvs FAPB2.3.6 WT and L1TAG—where L1 represents position 1 of the light chain[40, 42]). These results indicate that only the display of full-length sdAbs results in binding to LC/A, and that ncAA incorporation at these sites does not abolish interactions between the proteins.

To further characterize the effect of the ncAAs on binding, we selected two sdAbs for quantitative examination of binding affinity via titration of LC/A to a fixed concentration of sdAb displayed on yeast cells.[43] We limited this analysis to AzF-containing clones, as spontaneous crosslinking from OBeY would not be expected to follow the standard behavior of reversible binding events and prevent determination of affinity constants. We chose JPU-A5 N54AzF and JPU-C1 L101AzF as they showed promising photoreactivity in our initial screening (see Photocrosslinking section below), as well as their parent WT counterparts for comparison. Titrations were carried out with a fixed concentration of induced cells and varying concentrations of LC/A, with unbound LC/A removed before fluorescent labeling for flow cytometry. The apparent dissociation constant ($K_{d,\ app}$) values were then estimated by fitting to a one-site binding model as shown in Figure 2c (see Materials and Methods for details). The resulting $K_{d,\ app}$ values of AzF mutants were comparable to the $K_{d,\ app}$ values of the corresponding WT sdAbs, providing further evidence that ncAA incorporation does not significantly impair binding to the target.

Taken as a whole, the observed LC/A binding retention indicates that numerous ncAA substitutions in this series of sdAbs are well-tolerated. Particularly, in the case of the JPU-A5 N54AzF and JPU-C1 L101AzF mutants, the substitutions do not appear to alter apparent binding affinities under the conditions used here. Both the streamlined investigation of more than 40 distinct variants on the yeast surface and the tolerances for ncAA substitutions observed here indicate the feasibility of preparing and characterizing large collections of ncAA-expanded proteins in yeast display format. Having confidence that our series of ncAA-substituted variants retain binding toward LC/A, we moved on to using our platform to identify sdAb candidates capable of crosslinking to LC/A either after UV exposure (in the case of AzF) or spontaneously (in the case of OBeY).

3.3 Photocrosslinking with AzF

AzF has been used extensively for its reactivity upon exposure to UV light and has been particularly useful to explore the molecular underpinnings of protein-protein interactions.[16, 18–21, 45, 46] Our group has recently shown that photocrosslinking between scFvs incorporating AzF and their binding partners can be studied on the yeast surface.[22]

Thus, we analyzed our collection of AzF-containing sdAbs to find positions that would result in covalent crosslinking events with LC/A.

We reasoned that subjecting noncovalent LC/A-sdAb complexes on the yeast surface to stringent denaturation conditions would result in dissociation of the LC/A, while covalent complexes would remain detectable via flow cytometry. To achieve this, yeast cells displaying AzF-substituted sdAbs were incubated with LC/A, irradiated with 365 nm UV light, washed to remove unbound LC/A, and incubated under denaturing conditions (8 M urea, 200 mM EDTA, 20 mM Tris, pH 8.0) before labeling and analysis via flow cytometry (Figure 3a; see Materials and Methods for details). Fluorescence levels corresponding to LC/A detection after this process for all variants evaluated in this study are depicted in Figure 3b. As expected, yeast displaying WT constructs exhibited background levels of fluorescence after treatment with denaturant (Figure S6). Additionally, control non-binding proteins M0076 and DX-2802 (scFvs, both WT and L1AzF–where L1 represents position 1 of the light chain),[47, 48] also exhibited background levels of fluorescence following crosslinking and denaturation, indicating that the presence of AzF in proteins displayed on the yeast surface is not sufficient to retain LC/A after denaturation. In contrast, many AzF-substituted mutants showed elevated LC/A detection levels, strongly suggesting the occurrence of crosslinking events. While it is tempting to assume that LC/A detection levels after crosslinking are an indicator of crosslinking efficiency, construct-specific changes in affinity and display levels upon AzF substitution make this a potentially risky assumption. Based on previous structural studies[49] that show a relationship between C–C distances, we investigated whether Cα–Cα distance was a predictor of observed crosslinking activity. Plotting putative crosslinking level versus Cα-Cα distance between the mutated amino acid and its nearest LC/A residue revealed no distinct correlation between detected LC/A levels and the distances (Figure S8). Given the possibility of a reactive electrophile species deriving from photoactivation of AzF,[18, 50] we also compared the apparent crosslinking levels against the Cα-Cα distance to the nearest LC/A nucleophile, resulting in a similar plot without a clear correlation between the two variables (Figure S8a). Interestingly, even positions that appear to be distant from the sdAb-LC/A interface (JPU-A5 Q1; JPU-C10 Q1 and Q44; ciA-H7 Q1) showed some degree of apparent photocrosslinking. It is possible that dynamic protein motions could lead to successful crosslinking, or that LC/A multimerization or aggregation brings other LC/A molecules within proximity of distal portions of the sdAbs. However, we also determined that crosslinking assays conducted using a low-power handheld UV lamp (Figures S9, S10) did not show detectable levels of crosslinking at these locations; this suggests that photocrosslinking at the most distant sites from the target occurs with only low frequencies. In any case, distance between residues located on the two proteins alone seems to be a poor predictor of target crosslinking.

To better characterize putatively crosslinkable sdAb variants, we studied the time-dependent behavior of two promising candidates: JPU-A5 N54AzF and JPU-C1 L101AzF. JPU-A5 N54AzF was chosen due to its apparently high target crosslinking levels (Figure 3b). While the JPU-C1 L101AzF clone exhibits lower crosslinking levels than those of some other variants in the data shown in Figure 3b, high crosslinking levels in a preliminary study with a handheld lamp prompted us to choose this particular mutant for further investigation (Figures S9, S10). To conduct time course experiments, displayed sdAbs were treated

with LC/A in the dark and irradiated for times between 0 and 5 minutes, with aliquots taken at several time intervals (Figures 3c, d, S11). The binding control experiments, i.e. without the denaturation step, confirm the ability of the displayed clones to bind to the LC/A. Furthermore, no LC/A was detected in non-irradiated samples (0 time) after denaturation, indicating that reactivity is dependent on irradiation. The signal corresponding to LC/A increased in an irradiation time-dependent fashion for the AzF-containing clones but remained low for the WT constructs (Figure 3d, S11). Taken together, these results provide strong evidence that AzF is required to retain LC/A on the yeast surface, which we attribute to a covalent interaction formed between the sdAb and the LC/A. Interestingly, the detected MFI levels of LC/A (Figure 3d) stabilize after 3 minutes of irradiation without reaching the same levels of the binding control (Figure S12), suggesting that not all binding events result in covalent interactions. This could be attributable to the fast decay of the nitrene intermediate species into a less reactive electrophile,[18] resulting in decreased the yield of crosslinked adducts.[22, 50–52]

Overall, these studies demonstrate the extended range of photocrosslinking assays that can be conducted on the yeast surface. Conducting harsh denaturation steps and time courses in display format make it feasible to conduct early-stage mutant characterizations without the need to conduct solution-phase assays. With these proof-of-concepts in hand, we sought to extend these capabilities to the discovery of spontaneously crosslinkable sdAb variants on the yeast surface.

3.4 Spontaneous crosslinking with OBeY

While photocrosslinking has been a powerful tool for studying interactions in vitro, functional groups that require activation with short wavelengths of light are not necessarily amenable to in vivo applications. With this in mind, we investigated whether any of our mutants, albeit primarily designed for photocrosslinking with AzF, could support spontaneous crosslinking with OBeY. The latter ncAA contains an electrophilic bromoethyl chain that has been used for targeting nearby nucleophilic residues, particularly the thiol side chain of cysteine.[24, 53, 54]

We used a scheme similar to the one described for photocrosslinking studies to screen for OBeY mutants capable of forming covalent adducts on the yeast surface (Figure 4a). The crosslinking was promoted by incubating displaying cells with LC/A for 24 h at 37 °C. Excess LC/A was then removed by washing, and cells were subjected to denaturing conditions to remove noncovalently bound LC/A. Figure 4b shows LC/A fluorescence detection levels after flow cytometry analysis. Installing OBeY at the same positions used for AzF mutants, substitution sites that appeared to facilitate spontaneous crosslinking with OBeY (Figure 4b; based on LC/A levels above those of their corresponding WT versions) were different than those found with AzF mutants (Figure 3b). Specifically, JPU-A5 Y101OBeY, JPU-C1 Y32OBeY, and JPU-C1 M104OBeY mutants appeared to promote spontaneous crosslinking.

As in the case of photocrosslinking, the results did not show any clear correlation between crosslinking and Cα–Cα distance between the mutated residue and the most proximal Cα in LC/A (Figure S8b). A similar analysis involving the nearest LC/A nucleophile revealed

that that crosslinking only occurred with Cα–Cα distances between 8–10 Å, although not all mutants with a nucleophilic residue at this distance showed evidence of spontaneous crosslinking (Figure S8b). Since alkyl halides have been shown to react with diverse nucleophiles present in proteins[55, 56], we also systematically examined the Cα distances to each type of reactive nucleophile in LC/A (Figure S8c). No discernible correlation was observed between crosslinking and distance for most nucleophiles. However, the plots corresponding to the nearest LC/A Cys or His residue show that higher levels of LC/A detection may be related to proximity to these residues, hinting at the possible identity of the reactive site in LC/A. While these trends indicate that distance to these nucleophiles is an important factor to consider in the positioning of reactive ncAAs, not all substitutions that satisfy this distance requirement resulted in detectable LC/A levels, indicating that other factors must come into play to achieve spontaneous covalent engagement.

To corroborate these findings, we monitored retention of LC/A on the yeast surface after incubation with the target for different time intervals followed by denaturation. To account for the possibility that new noncovalent interactions arising from OBeY substitution led to enhanced binding (or hinder denaturation and dissociation from the yeast surface), we included sdAbs incorporating the alkyne-containing ncAA *O*-propargyltyrosine (OPG) in place of OBeY as controls. OPG structurally resembles OBeY while lacking the reactive electrophilic center; it can also be incorporated into proteins in yeast using the AcFRS OTS.[40]

Figure 4c depicts flow cytometry dot plots of yeast display samples analyzed after incubation for 1 and 24 h followed by removal of noncovalently bound LC/A. These plots qualitatively indicate that OBeY-containing proteins retain substantial binding to LC/A after denaturation. In contrast, the WT and OPG-containing constructs show binding to LC/A but reduced or no retention after denaturation, suggesting that the reactive 2-bromoethyl chain of OBeY is necessary to retain binding following denaturation.

Quantitative evaluations of LC/A detection levels following a range of incubation times and standard denaturation (Figure 4d) indicate a clear time dependence of the amount of LC/A retained on the yeast surface, with detectable increases in LC/A levels observed within the first several hours with OBeY-substituted clones. Only after times of 6 h or longer do we begin to detect LC/A in some control samples. The comparatively short time scales over which LC/A levels rise in OBeY-substituted samples and relatively low background levels of LC/A detected for controls under similar conditions are consistent with the notion of spontaneous covalent interaction formation mediated by OBeY.

After long incubation times, yeast displaying JPU-A5 WT or JPU-C1 M104OPG-containing clones exhibit low but detectable levels of LC/A. While we are unsure of the exact mechanism that leads to this phenomenon, it is possible that long-term incubation of LC/A in the presence of yeast leads to aggregation or other conformationally altered states that are difficult to remove with denaturation procedures. Additionally, recent reports show that terminal alkynes, such as the one present in OPG, can engage in covalent interactions with cysteines via proximity-enhanced reactivity.[57, 58] Given the proximity between position 104

in the JPU-C1 sdAb to LC/A Cys165, this could account for some of the LC/A retention in the case of M104OPG.

These results further highlight the robustness of yeast display as a platform for the discovery of covalent antibodies, here promoted by proximity-enhanced crosslinking. Thus, our yeast display platform supports systematic evaluations that support the identification of multiple types of putative covalent interactions prior to the production of promising soluble candidates for solution-phase characterization.

3.5 In-solution crosslinking characterizations

Given our success in identifying covalent antibodies on the yeast surface, we sought to corroborate our findings in soluble form. We cloned sdAb genes and TAG-containing variants into a modified version of pRS314 that serves as a secretion vector and incorporates C-terminal hexahistidine and cMyc tags into the encoded constructs.[59, 60] Here, we focused our characterizations on the L101AzF, Y32OBeY, and M104OBeY derivatives of JPU-C1, which could be expressed at levels sufficient to facilitate solution-phase assays. The purities and concentrations of all soluble sdAbs were evaluated using SDS-PAGE analysis. In addition to the functional data presented in the studies below, characterizations via bioorthogonal chemistry and MALDI-TOF mass spectrometry[61–63] provided direct evidence for ncAA incorporation in the L101AzF and Y32OBeY clones, respectively (see Materials and Methods and Figure S16 for details).

Following expression and purification of all derivatives, we sought to determine the crosslinking properties of the soluble sdAb variants. Photocrosslinking was attempted by incubating either the WT or L101AzF sdAbs in the presence of LC/A followed by UV irradiation of the samples in a photoreactor for 2 min. Spontaneous crosslinking was attempted by incubating WT, Y32OBeY, or M104OBeY with LC/A at 37 °C for 24 h. Analysis was carried out via SDS-PAGE, as the denaturing conditions disrupt noncovalent interactions between the sdAb and the LC/A, and covalent adducts are detected as a new band with increased molecular weight.

Figures 5a and 5b show the gel images resulting from photocrosslinking and spontaneous crosslinking experiments, respectively (see Figure S17 and S18 for complete gel and blot images). In both sets of experiments, when LC/A was incubated with WT sdAb only the bands corresponding to each separate protein were visible after Coomassie staining. However, when LC/A was incubated with ncAA-containing sdAbs in their corresponding conditions (irradiation for 2 min or 24 h incubation), we detected an additional band of a molecular weight consistent with the expected size of the LC/A-sdAb adduct. Densitometric analysis revealed that the band intensities for the crosslinked adducts were 38.1 ± 2.9% (L101AzF), 35.5 ± 4.4% (Y32OBeY) and 38.1 ± 5.7% (M104OBeY) when compared to the non-reconstituted LC/A control. These values represent an upper-limit estimate of the crosslinking yield under the experimental conditions used here, as LC/A degradation, differences in staining of different molecular weight proteins, and signal saturation limit the accuracy of this calculation.

In order to confirm the composition of the presumptive adducts, we took advantage of the C-terminal tags present in LC/A (Strep-tag) and the sdAbs (cMyc). Using western blots with the two different detection antibodies, we observed that this high-molecular weight band was observed when probing for both tags, validating its identity (Figures 5a, b, S17, S18). Additionally, the western blot for the cMyc epitope revealed bands at approximately 50 kDa when LC/A was incubated with the OBeY-containing sdAbs. The sizes of these bands are consistent with a crosslinked adduct between the sdAb and a previously reported ~35 kDa N-terminal degradation product of LC/A.[64, 65] This observation further corroborates the reactivity between the LC/A and sdAbs, while also providing evidence regarding the crosslinking position on the LC/A. Since the ~35 kDa corresponds to the 250-residue, N-terminal portion of the protease,[64, 65] we infer that crosslinking occurs between the sdAb and amino acid(s) in the range of residues 1–249 of LC/A. This in line with the crystallographic data, which shows that interactions between WT JPU C1 and LC/A occur within this domain.[38]

With convincing evidence for crosslinking interactions in solution, we next sought to evaluate covalent adduct formation as a function of time. SDS-PAGE analysis facilitated characterization of the formation of the photocrosslinked LC/A-sdAb adduct for varying irradiation times. The results in Figures 5c, d indicate that the intensity of the band corresponding to the LC/A-JPU-C1 L101AzF complex increased until reaching a maximum after 3 minutes of irradiation, consistent with the observed increase in covalently bound LC/A detected on the yeast surface (see Figure S19 for full image).

We conducted similar experiments with JPU-C1 M104OBeY by following adduct formation over time as well as at different pH values (Figure S20). Interestingly, the intensity of the crosslinked adduct increased over the first 12 h of incubation in buffer at pH 7.1, while increasing for only the first 8 h in buffers at pH values of 8.0 or 9.0 and yielding lower final quantities of adducts. This is surprising given that the bromoethyl functionality typically reacts with nucleophilic thiols or amines, and thus reactivity is expected to increase at high pH values. Alternatively, the distance analysis (Figure S8c) revealed the possibility of crosslinking to His residues, which may not show noticeable increases in nucleophilicity at the studied pH values. Furthermore, we also observed that LC/A autolysis was impaired at higher pH values (Figure S20a). Hence, decreased crosslinking at higher pH values may be attributable to structural changes in LC/A that hinder sdAb binding and thus interfere with covalent engagement.

The soluble characterizations performed here confirm the crosslinking capabilities of several sdAb variants initially identified on the yeast surface and indicate that crosslinking time scales are similar on yeast and in solution. These findings further validate the use of the yeast display format to conduct initial experiments prior to moving to solution-based assays.

3.6 Inhibitory properties of sdAbs

To better understand the properties of the soluble ncAA-sdAbs, we evaluated the inhibitory and selectivity properties of the clones. First, during the spontaneous crosslinking experiments performed in Figure 5b, we observed qualitative evidence suggesting that sdAb variants were preventing LC/A autoproteolysis. In the absence of sdAbs, the band intensity

corresponding to active LC/A decreased following prolonged incubations, and new bands appeared: one slightly below the intact LC/A, the next one at ~35 kDa, and two near the 25 kDa marker (Figure 5b). This pattern is consistent with previous reports evaluating the autoproteolysis of LC/A.[64, 65] Interestingly, when LC/A was incubated in the presence of WT or OBeY JPU-C1 sdAb variants, the band intensity corresponding to intact LC/A remained similar to the band intensity in non-reconstituted LC/A, while intensities of bands at sizes corresponding to degradation products were less evident. This strongly suggests that both WT and OBeY-containing sdAbs are capable of inhibiting the autoproteolytic activity of LC/A, implying that OBeY substitution does not overtly disrupt the demonstrated inhibitory properties of WT JPU-C1.[38]

To quantitatively characterize the inhibitory properties of all three ncAA-sdAb variants considered here, we used a commercial FRET-based LC/A substrate to monitor enzymatic activity over time. By monitoring changes in reporter fluorescence over time in mixtures of a fixed LC/A concentration and varying sdAb amounts, we were able to determine the initial rates of reaction. The rate in the presence of varying concentrations of inhibitors can then be correlated to the fractional LC/A activity by normalizing by the rate of enzyme in the absence of sdAb. Fitting these data to a dose-response model allowed us to estimate the IC_{50} values for each sdAb (Figure 6, S21). The results indicate that the sdAbs retain their inhibitory capabilities when incorporating these ncAAs, although JPU-C1 Y32OBeY shows a ~5-fold decrease in inhibitory potency when compared to WT JPU-C1. The residue at position 32 is tyrosine in each of JPU-A5, JPU-C1, and JPU-C10, which may indicate that Y32 is a preferred amino acid at this sdAb position. Substitutions at this position could affect antibody stability and thus binding affinity to LC/A, resulting in the decreased inhibitory potency of JPU-C1 Y32OBeY. On the other hand, positions L101 and M104 are located within the highly variable CDR3 loop and are therefore more likely to tolerate ncAA substitutions without loss of binding affinity or inhibitory potency. We also made numerous attempts to characterize the effect of crosslinking on inhibition using this assay. However, both the fast autoproteolysis of LC/A and its photodegradation when irradiated in the absence of sdAb prevented us from quantifying the effects of crosslinking events on enzymatic activity in solution. Nonetheless, in-solution inhibition assays confirmed that ncAA-substituted variants of JPU-C1 retain inhibitory properties.

3.7 Selectivity of ncAA-containing sdAbs

Having evaluated the behavior of our chemically reactive sdAbs under “ideal” biochemical conditions, we investigated their selectivity when used to bind LC/A in complex mixtures to determine whether the introduction of crosslinkable groups leads to detectable levels of off-target interactions. Here, we used mammalian cell lysates to present a range of potential intracellular off targets, as any potential BoNT protease inhibitor would need to exhibit selectivity in the neuronal cytosol to prevent off-target crosslinking, thus reducing efficacy and possibly causing harm. Starting with the photocrosslinkable JPU-C1 L101AzF sdAb, we performed photocrosslinking experiments with varying concentrations of sdAb in the presence of HepG2 cell lysate spiked with a fixed concentration of LC/A. The solutions were then transferred to nitrocellulose membranes and probed for the cMyc tag present in the sdAb.

Figure 7a shows the resulting blots before and after irradiating the samples for 30 s. A band near 37 kDa appears with similar intensity in all lysate-containing samples, which we attribute to a lysate protein that cross-reacts with our cMyc detection antibody (this also serves as an internal standard for evaluating sdAb selectivity). The appearance of the band corresponding to the LC/A-sdAb adduct (Figure S24a) is dependent on concentration and requires sample irradiation. This provides a strong indication that the presence of lysate does not prevent crosslinking between the intended binding partners. Furthermore, the expected crosslinked adduct represents the major new band formed following irradiation. In the presence of LC/A, the appearance of additional bands remains at close to undetectable levels, while in the absence of LC/A, new bands only appear at very high concentrations of sdAb after irradiation. The intensities of these bands are noticeably lower than the intensities of the LC/A adduct; detailed densitometry (Figure S25a) confirms all of these observations. These data indicate that the AzF-substituted sdAb exhibits high target selectivity even in a complex sample.

We performed similar experiments with the soluble OBeY-containing sdAbs JPU-C1 Y32OBeY and JPU-C1 M104OBeY. The sdAbs were incubated with HepG2 lysate, and some samples were spiked with LC/A. The blots shown in Figure 7b reveal the appearance of the LC/A-JPU-C1 Y32OBeY adduct with a concentration-dependent band at approximately 75 kDa (Figure S24b), as well as the adduct corresponding to partially hydrolyzed LC/A-JPU-C1 Y32OBeY complex near the 50 kDa marker. Notably, no other bands other than the internal control were detected in this assay (see Figure S25b for detailed densitometry), indicating again that the presence of foreign proteins does not prevent association and reaction between JPU-C1 Y32OBeY and LC/A. Importantly, JPU-C1 Y32OBeY does not show detectable levels of off-target protein binding under the conditions used here.

Finally, Figure 7c shows the results of blotting experiments with cell lysates performed with JPU-C1 M104OBeY. We were able to detect the crosslinked sdAb-LC/A adduct (~75 kDa) when blotting against the LC/A even at substoichiometric concentrations of sdAb, again demonstrating that the presence of foreign proteins does not preclude the efficient covalent interaction between them (Figure S24c). We also observed the appearance of an additional band slightly below the 75 kDa marker with increasing concentrations of M104OBeY in the absence of LC/A, suggesting an unintended reaction of the sdAb with a protein in the lysate. Furthermore, a few less intense bands in the 75–100 kDa range appeared following incubations at high concentrations of sdAb. While this is an indication of off-target interactions of this substituted sdAb, by comparing the intensity profiles in the absence and presence of LC/A via densitometry (Figure S25c), we noticed that the appearance of these side products in the presence of LC/A is suppressed, appearing only at sdAb concentrations similar to or greater than the concentration of the added LC/A. This suggests that the sdAb exhibits a distinct crosslinking preference for LC/A, although its selectivity is lower than the selectivity of the other soluble ncAA-sdAbs characterized here.

Overall, these assays indicate that ncAA-substituted clones retain their inhibitory properties and can further exhibit target selectivity, although the extent to which selectivity is observed appears to depend on the ncAA substitution site. Thus, chemically augmented sdAbs

initially identified on the yeast surface in this work employing two different chemistries exhibited crosslinking functionalities in solution while retaining inhibition and, in some cases, high target selectivity.

4. Conclusions

In this study, we leveraged the combination of yeast display and ncAAs to discover and characterize sdAbs capable of covalently binding their target in one of two ways: via irradiation with short-wavelength light or via proximity-induced reaction. Based on previous crystallographic data,[38, 39] we installed two reactive ncAAs, AzF (for photocrosslinking) and OBeY (for spontaneous crosslinking), at selected positions in four previously discovered sdAbs known to bind to the botulinum neurotoxin light chain A1. Conducting assays in yeast display format allowed for efficient flow cytometric characterization of more than 40 sdAb variants, all without protein purification, and revealed that sdAbs exhibit high functional tolerance toward single site substitution with ncAAs. We further determined that this approach streamlines the identification of crosslinkable candidates via flow cytometry, both to identify sites that facilitate crosslinking and to evaluate time-dependent behaviors of these interactions.

These investigations include what we believe is the first discovery of spontaneously crosslinkable binding agents in yeast display format. Our discoveries of covalent OBeY-sdAb variants were unexpected, as the sites investigated in this work were initially selected using the structural data with the goal of facilitating the introduction of photocrosslinkable ncAAs, not electrophilic ncAAs. Finally, solution-based experiments revealed that the sdAb variants JPU-C1 L101AzF, Y32OBeY, and M104OBeY exhibited clear crosslinking activity in solution, retained the inhibitory activity of the parent, and possessed moderate to high levels of selectivity for LC/A when tested in the presence of complex protein mixtures.

Although a known benefit of irreversible inhibition is enhancement of inhibitor potency, we recognize that converting inhibitors that already exhibit high potency (such as the parent sdAbs used in this work) into covalent inhibitors may not readily reveal enhanced potency under typical conditions used during in vitro enzyme inhibition assays. Nonetheless, covalent target engagement can be advantageous in the prevention of inhibitor dissociation from the target and reactivation of the target. In the case of BoNT, covalent inhibitors are desirable to permanently inactivate the light chain protease, which exhibits an exceptionally long-lived half-life (~months) in the intracellular space. This potential benefit and others will need to be evaluated in cellular or animal models of BoNT infection in future studies.

In order to gauge the success of our predicted reactive sdAb positions, we used structural data to estimate distances between sdAb and LC/A residues and then compared these values with the apparent reactivities of sdAb variants determined on the yeast surface. Interestingly, many of these analyses revealed no clear correlations when measuring distances to the closest residue or nucleophile; even the short distances to the nearest Cys or His residues noted in sdAb clones that spontaneously crosslink to LC/A do not unambiguously reveal a single crosslinking site on the target. Our observations indicate that distance measurements alone are insufficient for accurate prediction of which ncAA

substitutions will lead to crosslinking events (although it is likely that expression level variability between clones accounts for some differences in apparent crosslinking levels). This suggests that factors in addition to proximity between ncAA substitution sites and nucleophiles on the target play a role in covalent target engagement in ways that have yet to be elucidated. Unpredictable reactivity levels and a dearth of structural data highlight the utility of a yeast display platform, or other platforms in the high throughput technology space, to facilitate engineering and characterization of chemically expanded antibodies that exhibit high affinity and target selectivity. Larger datasets that include both crosslinking efficiency and crosslinking site(s) of antibody variants bearing crosslinkable groups are needed to enable data-driven approaches to covalent antibody engineering.[66–68]

Future endeavors using the yeast-display screening tools reported here can be complemented by mechanistic investigations of successful crosslinkable antibodies using mass spectrometry to identify crosslinking site(s)[25, 26, 50, 52, 69, 70]. Additionally, valuable information could be obtained from structural[49] characterization of purified adducts, such as identification of local environments within complexes that promote efficient crosslinking. Thus, increasing both the breadth and depth of studies with covalent antibodies will be paramount for establishing principles for covalent binding agent discovery.

Moving beyond characterizations, further improvement of our platform will enable us to leverage the high throughput capabilities of yeast display with libraries of ncAA-containing proteins. New and improved genetic code expansion tools in yeast[40, 42, 63, 71–73] make it feasible to combine established yeast display strategies with libraries encoding ncAAs bearing various reactive groups (e.g. fluorosulfates for SuFEX chemistry and various Michael acceptors)[23, 24, 26, 27, 31, 54, 70] or with ncAAs that facilitate conjugations with chemical warheads.[23, 26, 29, 30, 54, 70, 74] This powerful combination provides a wide range of opportunities for covalent antibody discovery. Our results show that the phenotype resulting from ncAA-mediated covalent bond formation can be assayed on the yeast surface, while prior work in yeast display format established high throughput screens to tune the efficiency and selectivity of covalent bond formation.[75] We envision that a platform for discovering and characterizing covalent antibodies will lead to applications of covalent protein binding agents in basic biomedical research, diagnostics, and drug discovery.

Supplementary Material

Refer to Web version on PubMed Central for supplementary material.

Acknowledgements

This project was supported by the National Institute of Health Award Number U01AI093504. The content of this work is responsibility solely of the authors and does not represent the views of the National Institute of Health. The authors also acknowledge R. Cook and A. Leshinsky from the Biopolymers and Proteomics Core at the Koch Institute at the Massachusetts Institute of Technology for their help with mass spectrometry experiments. The authors would like to thank R. Hershman for aid with mammalian cell culture and editing contributions, as well as B. Lino for editing and feedback.

8. References

1. Boder ET; Wittrup KD Yeast surface display for screening combinatorial polypeptide libraries. Nature Biotechnology 1997, 15 (6), 553–557. DOI: 10.1038/nbt0697-553.
2. Thie H; Voedisch B; Dübel S; Hust M; Schirrmann T Affinity Maturation by Phage Display. In Therapeutic Antibodies: Methods and Protocols, Dimitrov AS Ed.; Humana Press, 2009; pp 309–322.
3. Van Deventer JA; Wittrup KD Yeast Surface Display for Antibody Isolation: Library Construction, Library Screening, and Affinity Maturation. In Monoclonal Antibodies: Methods and Protocols, Ossipow V, Fischer N Eds.; Humana Press, 2014; pp 151–181.
4. Könning D; Kolmar H Beyond antibody engineering: directed evolution of alternative binding scaffolds and enzymes using yeast surface display. Microbial Cell Factories 2018, 17 (1), 32. DOI: 10.1186/s12934-018-0881-3. [PubMed: 29482656]
5. Rappazzo CG; Tse LV; Kaku CI; Wrapp D; Sakharkar M; Huang D; Deveau LM; Yockachonis TJ; Herbert AS; Battles MB; O'Brien CM; Brown ME; Geoghegan JC; Belk J; Peng L; Yang L; Hou Y; Scobey TD; Burton DR; Nemazee D; Dye JM; Voss JE; Gunn BM; McLellan JS; Baric RS; Gralinski LE; Walker LM Broad and potent activity against SARS-like viruses by an engineered human monoclonal antibody. Science 2021, 371 (6531), 823–829. DOI: 10.1126/science.abf4830. [PubMed: 33495307]
6. Brockmann E-C Selection of Stable scFv Antibodies by Phage Display. In Antibody Engineering: Methods and Protocols, Second Edition, Chames P Ed.; Humana Press, 2012; pp 123–144.
7. McConnell AD; Zhang X; Macomber JL; Chau B; Sheffer JC; Rahmanian S; Hare E; Spasojevic V; Horlick RA; King DJ; Bowers PM A general approach to antibody thermostabilization. mAbs 2014, 6 (5), 1274–1282. DOI: 10.4161/mabs.29680. [PubMed: 25517312]
8. Warszawski S; Borenstein Katz A; Lipsh R; Khmelnitsky L; Ben Nissan G; Javitt G; Dym O; Unger T; Knop O; Albeck S; Diskin R; Fass D; Sharon M; Fleishman SJ Optimizing antibody affinity and stability by the automated design of the variable light-heavy chain interfaces. PLOS Computational Biology 2019, 15 (8), e1007207. DOI: 10.1371/journal.pcbi.1007207. [PubMed: 31442220]
9. Wang T; Badran AH; Huang TP; Liu DR Continuous directed evolution of proteins with improved soluble expression. Nature Chemical Biology 2018, 14 (10), 972–980. DOI: 10.1038/s41589-018-0121-5. [PubMed: 30127387]
10. de Picciotto S; Dickson PM; Traxlmayr MW; Marques BS; Socher E; Zhao S; Cheung S; Kiefer JD; Wand AJ; Griffith LG; Imperiali B; Wittrup KD Design Principles for SuCESsFul Biosensors: Specific Fluorophore/Analyte Binding and Minimization of Fluorophore/Scaffold Interactions. Journal of Molecular Biology 2016, 428 (20), 4228–4241. DOI: 10.1016/j.jmb.2016.07.004. [PubMed: 27448945]
11. Klaus T; Deshmukh S pH-responsive antibodies for therapeutic applications. Journal of Biomedical Science 2021, 28 (1), 11. DOI: 10.1186/s12929-021-00709-7. [PubMed: 33482842]
12. Garuti L; Roberti M; Bottegoni G Irreversible protein kinase inhibitors. Current Medicinal Chemistry 2011, 18 (20), 2981–2994. DOI: 10.2174/092986711796391705 From NLM. [PubMed: 21651479]
13. Singh J; Petter RC; Baillie TA; Whitty A The resurgence of covalent drugs. Nature Reviews Drug Discovery 2011, 10 (4), 307–317. DOI: 10.1038/nrd3410. [PubMed: 21455239]
14. González-Bello C Designing Irreversible Inhibitors—Worth the Effort? ChemMedChem 2016, 11 (1), 22–30. DOI: 10.1002/cmdc.201500469. [PubMed: 26593241]
15. Sutanto F; Konstantinidou M; Dömling A Covalent inhibitors: a rational approach to drug discovery. RSC Medicinal Chemistry 2020, 11 (8), 876–884. DOI: 10.1039/D0MD00154F. [PubMed: 33479682]
16. Chin JW; Santoro SW; Martin AB; King DS; Wang L; Schultz PG Addition of p-Azido-L-phenylalanine to the Genetic Code of Escherichia coli. Journal of the American Chemical Society 2002, 124 (31), 9026–9027. DOI: 10.1021/ja027007w. [PubMed: 12148987]
17. Chin JW; Schultz PG In Vivo Photocrosslinking with Unnatural Amino Acid Mutagenesis. ChemBioChem 2002, 3 (11), 1135–1137. DOI: 10.1002/1439-7633(20021104)3:11<1135::AID-CBIC1135>3.0.CO;2-M. [PubMed: 12404640]

18. Preston GW; Wilson AJ Photo-induced covalent cross-linking for the analysis of biomolecular interactions. Chemical Society Reviews 2013, 42 (8), 3289–3301. DOI: 10.1039/C3CS35459H. [PubMed: 23396550]
19. Lancia JK; Nwokoye A; Dugan A; Joiner C; Pricer R; Mapp AK Sequence context and crosslinking mechanism affect the efficiency of in vivo capture of a protein-protein interaction. Biopolymers 2014, 101 (4), 391–397. DOI: 10.1002/bip.22395. [PubMed: 24037947]
20. Coin I Application of non-canonical crosslinking amino acids to study protein–protein interactions in live cells. Current Opinion in Chemical Biology 2018, 46, 156–163. DOI: 10.1016/j.cbpa.2018.07.019. [PubMed: 30077876]
21. Chen H; Wilson J; Ottinger S; Gan Q; Fan C Introducing noncanonical amino acids for studying and engineering bacterial microcompartments. Current Opinion in Microbiology 2021, 61, 67–72. DOI: 10.1016/j.mib.2021.03.004. [PubMed: 33813159]
22. Islam M; Kehoe HP; Lissoos JB; Huang M; Ghadban CE; Berumen Sánchez G; Lane HZ; Van Deventer JA Chemical Diversification of Simple Synthetic Antibodies. ACS Chemical Biology 2021, 16 (2), 344–359. DOI: 10.1021/acschembio.0c00865. [PubMed: 33482061]
23. Chen X-H; Xiang Z; Hu YS; Lacey VK; Cang H; Wang L Genetically Encoding an Electrophilic Amino Acid for Protein Stapling and Covalent Binding to Native Receptors. ACS Chemical Biology 2014, 9 (9), 1956–1961. DOI: 10.1021/cb500453a. [PubMed: 25010185]
24. Xiang Z; Lacey VK; Ren H; Xu J; Burban DJ; Jennings PA; Wang L Proximity-Enabled Protein Crosslinking through Genetically Encoding Haloalkane Unnatural Amino Acids. Angewandte Chemie International Edition 2014, 53 (8), 2190–2193. DOI: 10.1002/anie.201308794. [PubMed: 24449339]
25. Yang B; Wu H; Schnier PD; Liu Y; Liu J; Wang N; DeGrado WF; Wang L Proximity-enhanced SuFEx chemical cross-linker for specific and multitargeting cross-linking mass spectrometry. Proceedings of the National Academy of Sciences 2018, 115 (44), 11162–11167. DOI: 10.1073/pnas.1813574115.
26. Li Q; Chen Q; Klauser PC; Li M; Zheng F; Wang N; Li X; Zhang Q; Fu X; Wang Q; Xu Y; Wang L Developing Covalent Protein Drugs via Proximity-Enabled Reactive Therapeutics. Cell 2020, 182 (1), 85–97.e16. DOI: 10.1016/j.cell.2020.05.028. [PubMed: 32579975]
27. Cheng Y; Wu J; Han Y; Xu J; Da Y; Zhao Q; Guo G; Zhou Y; Chen Y; Liu J; Chen H; Jiang X; Cai X A CDR-based approach to generate covalent inhibitory antibody for human rhinovirus protease. Bioorganic & Medicinal Chemistry 2021, 42, 116219. DOI: 10.1016/j.bmc.2021.116219. [PubMed: 34077853]
28. Zhang H; Han Y; Yang Y; Lin F; Li K; Kong L; Liu H; Dang Y; Lin J; Chen PR Covalently Engineered Nanobody Chimeras for Targeted Membrane Protein Degradation. Journal of the American Chemical Society 2021, 143 (40), 16377–16382. DOI: 10.1021/jacs.1c08521. [PubMed: 34596400]
29. McCarthy KA; Kelly MA; Li K; Cambray S; Hosseini AS; van Opijnen T; Gao J Phage Display of Dynamic Covalent Binding Motifs Enables Facile Development of Targeted Antibiotics. Journal of the American Chemical Society 2018, 140 (19), 6137–6145. DOI: 10.1021/jacs.8b02461. [PubMed: 29701966]
30. Chen S; Lovell S; Lee S; Fellner M; Mace PD; Bogyo M Identification of highly selective covalent inhibitors by phage display. Nature Biotechnology 2021, 39 (4), 490–498. DOI: 10.1038/s41587-020-0733-7.
31. Liu CC; Mack AV; Brustad EM; Mills JH; Groff D; Smider VV; Schultz PG Evolution of Proteins with Genetically Encoded “Chemical Warheads”. Journal of the American Chemical Society 2009, 131 (28), 9616–9617. DOI: 10.1021/ja902985e. [PubMed: 19555063]
32. Garland M; Babin BM; Miyashita S-I; Loscher S; Shen Y; Dong M; Bogyo M Covalent Modifiers of Botulinum Neurotoxin Counteract Toxin Persistence. ACS Chemical Biology 2019, 14 (1), 76–87. DOI: 10.1021/acschembio.8b00937. [PubMed: 30571080]
33. Lin L; Olson ME; Eubanks LM; Janda KD Strategies to Counteract Botulinum Neurotoxin A: Nature’s Deadliest Biomolecule. Accounts of chemical research 2019, 52 (8), 2322–2331. DOI: 10.1021/acs.accounts.9b00261. [PubMed: 31322847]

34. Lin L; Olson ME; Sugane T; Turner LD; Tararina MA; Nielsen AL; Kurbanov EK; Pellett S; Johnson EA; Cohen SM; Allen KN; Janda KD Catch and Anchor Approach To Combat Both Toxicity and Longevity of Botulinum Toxin A. Journal of Medicinal Chemistry 2020, 63 (19), 11100–11120. DOI: 10.1021/acs.jmedchem.0c01006. [PubMed: 32886509]
35. Turner LD; Nielsen AL; Lin L; Pellett S; Sugane T; Olson ME; Johnson EA; Janda KD Irreversible inhibition of BoNT/A protease: proximity-driven reactivity contingent upon a bifunctional approach. RSC Medicinal Chemistry 2021, 12 (6), 960–969. DOI: 10.1039/D1MD00089F. [PubMed: 34223161]
36. McNutt PM; Vazquez-Cintron EJ; Tenezaca L; Ondeck CA; Kelly KE; Mangkhalakhili M; Machamer JB; Angeles CA; Glotfelty EJ; Cika J; Benjumea CH; Whitfield JT; Band PA; Shoemaker CB; Ichtchenko K Neuronal delivery of antibodies has therapeutic effects in animal models of botulism. Science Translational Medicine 2021, 13 (575), eabd7789. DOI: 10.1126/scitranslmed.abd7789. [PubMed: 33408188]
37. Miyashita S-I; Zhang J; Zhang S; Shoemaker CB; Dong M Delivery of single-domain antibodies into neurons using a chimeric toxin-based platform is therapeutic in mouse models of botulism. Science Translational Medicine 2021, 13 (575), eaaz4197. DOI: 10.1126/scitranslmed.aaz4197. [PubMed: 33408184]
38. Lam K.-h.; Tremblay JM; Perry K; Ichtchenko K; Shoemaker CB; Jin R Probing the structure and function of the protease domain of botulinum neurotoxins using single-domain antibodies. PLOS Pathogens 2022, 18 (1), e1010169. DOI: 10.1371/journal.ppat.1010169. [PubMed: 34990480]
39. Lam K.-h.; Tremblay JM; Vazquez-Cintron E; Perry K; Ondeck C; Webb RP; McNutt PM; Shoemaker CB; Jin R Structural Insights into Rational Design of Single-Domain Antibody-Based Antitoxins against Botulinum Neurotoxins. Cell Reports 2020, 30 (8), 2526–2539.e2526. DOI: 10.1016/j.celrep.2020.01.107. [PubMed: 32101733]
40. Stieglitz JT; Kehoe HP; Lei M; Van Deventer JA A Robust and Quantitative Reporter System To Evaluate Noncanonical Amino Acid Incorporation in Yeast. ACS Synthetic Biology 2018, 7 (9), 2256–2269. DOI: 10.1021/acssynbio.8b00260. [PubMed: 30139255]
41. Van Deventer JA; Le DN; Zhao J; Kehoe HP; Kelly RL A platform for constructing, evaluating, and screening bioconjugates on the yeast surface. Protein Engineering, Design and Selection 2016, 29 (11), 485–494. DOI: 10.1093/protein/gzw029.
42. Potts KA; Stieglitz JT; Lei M; Van Deventer JA Reporter system architecture affects measurements of noncanonical amino acid incorporation efficiency and fidelity. Molecular Systems Design & Engineering 2020, 5 (2), 573–588. DOI: 10.1039/C9ME00107G. [PubMed: 33791108]
43. Chao G; Lau WL; Hackel BJ; Sazinsky SL; Lippow SM; Wittrup KD Isolating and engineering human antibodies using yeast surface display. Nature Protocols 2006, 1 (2), 755–768. DOI: 10.1038/nprot.2006.94. [PubMed: 17406305]
44. Van Deventer JA; Kelly RL; Rajan S; Wittrup KD; Sidhu SS A switchable yeast display/secretion system. Protein Engineering, Design and Selection 2015, 28 (10), 317–325. DOI: 10.1093/protein/gzv043.
45. Rimbault C; Maruthi K; Breillat C; Genuer C; Crespillo S; Puente-Muñoz V; Chamma I; Gauthereau I; Antoine S; Thibaut C; Tai FWJ; Dartigues B; Grillo-Bosch D; Claverol S; Poujol C; Choquet D; Mackereth CD; Sainlos M Engineering selective competitors for the discrimination of highly conserved protein-protein interaction modules. Nature Communications 2019, 10 (1), 4521. DOI: 10.1038/s41467-019-12528-4.
46. Neumann H; Neumann-Staubitz P; Witte A; Summerer D Epigenetic chromatin modification by amber suppression technology. Current Opinion in Chemical Biology 2018, 45, 1–9. DOI: 10.1016/j.cbpa.2018.01.017. [PubMed: 29452937]
47. Nicholson S; Wood C; Devy L Use of mmp-9 and mmp-12 binding proteins for the treatment and prevention of systemic sclerosis WO 2010/045388 A2, 2010.
48. Wood CR Combination treatments comprising protease binding proteins for inflammatory disorders Canada CA 2741492 A1, 2009.
49. Sato S; Mimasu S; Sato A; Hino N; Sakamoto K; Umehara T; Yokoyama S Crystallographic Study of a Site-Specifically Cross-Linked Protein Complex with a Genetically Incorporated Photoreactive Amino Acid. Biochemistry 2011, 50 (2), 250–257. DOI: 10.1021/bi1016183. [PubMed: 21128684]

50. Nguyen T-A; Cigler M; Lang K Expanding the Genetic Code to Study Protein–Protein Interactions. Angewandte Chemie International Edition 2018, 57 (44), 14350–14361. DOI: 10.1002/anie.201805869. [PubMed: 30144241]
51. Futran AS; Kyin S; Shvartsman SY; Link AJ Mapping the binding interface of ERK and transcriptional repressor Capicua using photocrosslinking. Proceedings of the National Academy of Sciences 2015, 112 (28), 8590–8595. DOI: 10.1073/pnas.1501373112.
52. Yang B; Tang S; Ma C; Li S-T; Shao G-C; Dang B; DeGrado WF; Dong M-Q; Wang PG; Ding S; Wang L Spontaneous and specific chemical cross-linking in live cells to capture and identify protein interactions. Nature Communications 2017, 8 (1), 2240. DOI: 10.1038/s41467-017-02409-z.
53. Tang H; Dai Z; Qin X; Cai W; Hu L; Huang Y; Cao W; Yang F; Wang C; Liu T Proteomic Identification of Protein Tyrosine Phosphatase and Substrate Interactions in Living Mammalian Cells by Genetic Encoding of Irreversible Enzyme Inhibitors. Journal of the American Chemical Society 2018, 140 (41), 13253–13259. DOI: 10.1021/jacs.8b06922. [PubMed: 30247891]
54. Wang N; Wang L Genetically encoding latent bioreactive amino acids and the development of covalent protein drugs. Current Opinion in Chemical Biology 2022, 66, 102106. DOI: 10.1016/j.cbpa.2021.102106. [PubMed: 34968810]
55. Kramer JR; Deming TJ Reversible chemoselective tagging and functionalization of methionine containing peptides. Chemical Communications 2013, 49 (45), 5144–5146. DOI: 10.1039/C3CC42214C. [PubMed: 23629584]
56. Shu X; Asghar S; Yang F; Li S-T; Wu H; Yang B Uncover New Reactivity of Genetically Encoded Alkyl Bromide Non-Canonical Amino Acids. Frontiers in Chemistry 2022, 10. DOI: 10.3389/fchem.2022.815991.
57. Mons E; Jansen IDC; Loboda J; van Doodewaerd BR; Hermans J; Verdoes M; van Boeckel CAA; van Veelen PA; Turk B; Turk D; Ovaa H The Alkyne Moiety as a Latent Electrophile in Irreversible Covalent Small Molecule Inhibitors of Cathepsin K. Journal of the American Chemical Society 2019, 141 (8), 3507–3514. DOI: 10.1021/jacs.8b11027. [PubMed: 30689386]
58. Mons E; Kim RQ; van Doodewaerd BR; van Veelen PA; Mulder MPC; Ovaa H Exploring the Versatility of the Covalent Thiol–Alkyne Reaction with Substituted Propargyl Warheads: A Deciding Role for the Cysteine Protease. Journal of the American Chemical Society 2021, 143 (17), 6423–6433. DOI: 10.1021/jacs.0c10513. [PubMed: 33885283]
59. Shusta EV; Raines RT; Plückthun A; Wittrup KD Increasing the secretory capacity of Saccharomyces cerevisiae for production of single-chain antibody fragments. Nature Biotechnology 1998, 16 (8), 773–777. DOI: 10.1038/nbt0898-773.
60. Sikorski RS; Hieter P A system of shuttle vectors and yeast host strains designed for efficient manipulation of DNA in Saccharomyces cerevisiae. Genetics 1989, 122 (1), 19–27. DOI: 10.1093/genetics/122.1.19. [PubMed: 2659436]
61. Fang KY; Lieblich SA; Tirrell DA Incorporation of Non-Canonical Amino Acids into Proteins by Global Reassignment of Sense Codons. In Protein Scaffolds: Design, Synthesis, and Applications, Udit AK Ed.; Springer New York, 2018; pp 173–186.
62. Yang A; Ha S; Ahn J; Kim R; Kim S; Lee Y; Kim J; Söll D; Lee H-Y; Park H-S A chemical biology route to site-specific authentic protein modifications. Science 2016, 354 (6312), 623–626. DOI: doi:10.1126/science.aah4428. [PubMed: 27708052]
63. Stieglitz JT; Van Deventer JA High-Throughput Aminoacyl-tRNA Synthetase Engineering for Genetic Code Expansion in Yeast. ACS Synthetic Biology 2022, 11 (7), 2284–2299. DOI: 10.1021/acssynbio.1c00626. [PubMed: 35793554]
64. Ahmed SA; Byrne MP; Jensen M; Hines HB; Brueggemann E; Smith LA Enzymatic Autocatalysis of Botulinum A Neurotoxin Light Chain. Journal of Protein Chemistry 2001, 20 (3), 221–231. DOI: 10.1023/A:1010952025677. [PubMed: 11565902]
65. Segelke B; Knapp M; Kadkhodayan S; Balhorn R; Rupp B Crystal structure of Clostridium botulinum neurotoxin protease in a product-bound state: Evidence for noncanonical zinc protease activity. Proceedings of the National Academy of Sciences 2004, 101 (18), 6888–6893. DOI: 10.1073/pnas.0400584101.

66. Cao L; Coventry B; Goreshnik I; Huang B; Sheffler W; Park JS; Jude KM; Marković I; Kadam RU; Verschueren KHG; Verstraete K; Walsh STR; Bennett N; Phal A; Yang A; Kozodoy L; DeWitt M; Picton L; Miller L; Strauch E-M; DeBouver ND; Pires A; Bera AK; Halabiya S; Hammerson B; Yang W; Bernard S; Stewart L; Wilson IA; Ruohola-Baker H; Schlessinger J; Lee S; Savvides SN; Garcia KC; Baker D Design of protein-binding proteins from the target structure alone. Nature 2022, 605 (7910), 551–560. DOI: 10.1038/s41586-022-04654-9. [PubMed: 35332283]

67. Baek M; Baker D Deep learning and protein structure modeling. Nature Methods 2022, 19 (1), 13–14. DOI: 10.1038/s41592-021-01360-8. [PubMed: 35017724]

68. Xu J; Tack D; Hughes RA; Ellington AD; Gray JJ Structure-based non-canonical amino acid design to covalently crosslink an antibody–antigen complex. Journal of Structural Biology 2014, 185 (2), 215–222. DOI: 10.1016/j.jsb.2013.05.003. [PubMed: 23680795]

69. Zhang M; McEwen JM; Sjoblom NM; Kotewicz KM; Isberg RR; Scheck RA Members of the Legionella pneumophila Sde family target tyrosine residues for phosphoribosyl-linked ubiquitination. RSC Chemical Biology 2021, 2 (5), 1509–1519. DOI: 10.1039/D1CB00088H. [PubMed: 34704056]

70. Liu J; Cao L; Klauser PC; Cheng R; Berdan VY; Sun W; Wang N; Ghelichkhani F; Yu B; Rozovsky S; Wang L A Genetically Encoded Fluorosulfonyloxybenzoyl-L-lysine for Expansive Covalent Bonding of Proteins via SuFEx Chemistry. Journal of the American Chemical Society 2021, 143 (27), 10341–10351. DOI: 10.1021/jacs.1c04259. [PubMed: 34213894]

71. Hershman RL; Rezhdo A; Stieglitz JT; Van Deventer JA Engineering Proteins Containing Noncanonical Amino Acids on the Yeast Surface. In Yeast Surface Display, Traxlmayr MW Ed.; Springer US, 2022; pp 491–559.

72. Stieglitz JT; Van Deventer JA Incorporating, Quantifying, and Leveraging Noncanonical Amino Acids in Yeast. In Biomedical Engineering Technologies: Volume 2, Rasooly A, Baker H, Ossandon MR Eds.; Springer US, 2022; pp 377–432.

73. Stieglitz JT; Lahiri P; Stout MI; Van Deventer JA Exploration of Methanomethylophilus alvus Pyrrolysyl-tRNA Synthetase Activity in Yeast. ACS Synthetic Biology 2022, 11 (5), 1824–1834. DOI: 10.1021/acssynbio.2c00001. [PubMed: 35417129]

74. Ekanayake AI; Sobze L; Kelich P; Youk J; Bennett NJ; Mukherjee R; Bhardwaj A; Wuest F; Vukovic L; Derda R Genetically Encoded Fragment-Based Discovery from Phage-Displayed Macrocyclic Libraries with Genetically Encoded Unnatural Pharmacophores. Journal of the American Chemical Society 2021, 143 (14), 5497–5507. DOI: 10.1021/jacs.1c01186. [PubMed: 33784084]

75. Podracky CJ; An C; DeSousa A; Dorr BM; Walsh DM; Liu DR Laboratory evolution of a sortase enzyme that modifies amyloid-β protein. Nature Chemical Biology 2021, 17 (3), 317–325. DOI: 10.1038/s41589-020-00706-1. [PubMed: 33432237]

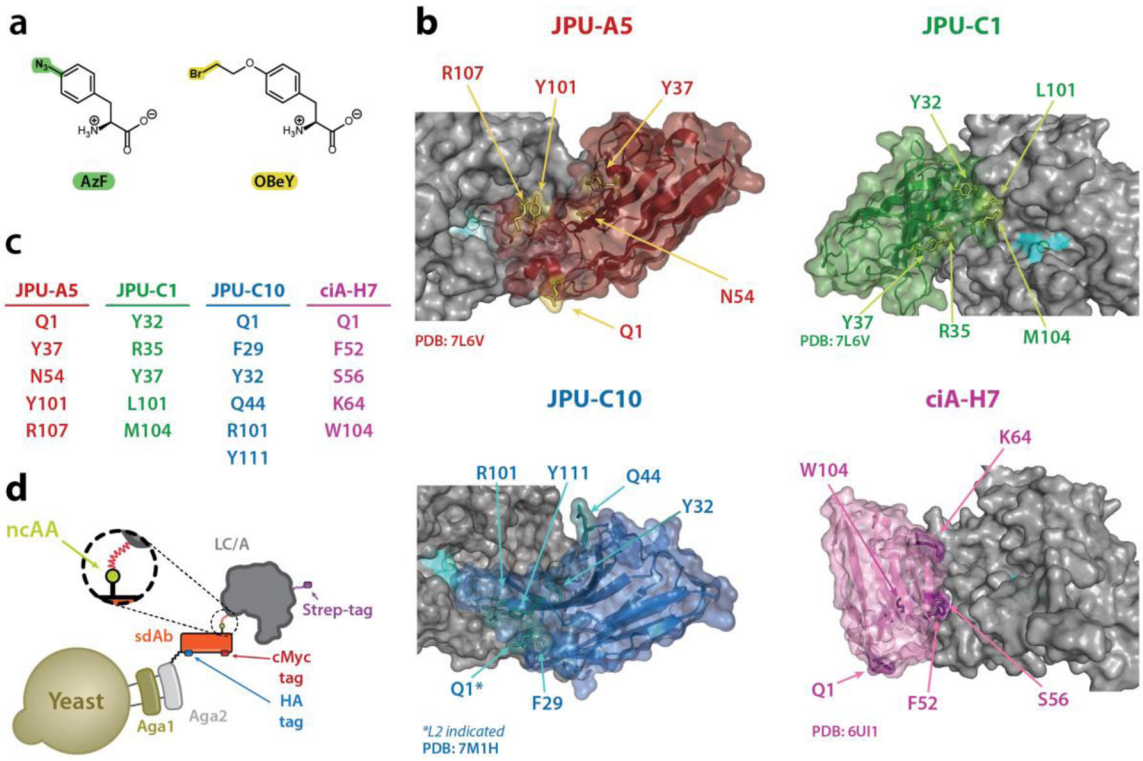

Figure 1.

Overview of strategy for presenting covalent functionalities in single-domain camelid antibodies targeting the light chain of botulinum neurotoxin serotype A1. **a** Reactive noncanonical amino acids used in this work for photocrosslinking (4-azido-L-phenylalanine; AzF) and spontaneous crosslinking (*O*-(2-bromoethyl)-L-tyrosine; OBeY). **b** Crystal structures of LC/A (gray surface, active site highlighted in cyan with catalytic Zn^{2+} shown as a sphere) bound to each wild type sdAb (shown as colored cartoons and transparent surfaces). The mutated residues are indicated and highlighted as sticks. **c** Residue positions used for ncAA incorporation in each of the four sdAbs used in this study. **d** Representation of strategy to evaluate ncAA-mediated covalent interactions between LC/A (shown in gray) and displayed sdAbs.

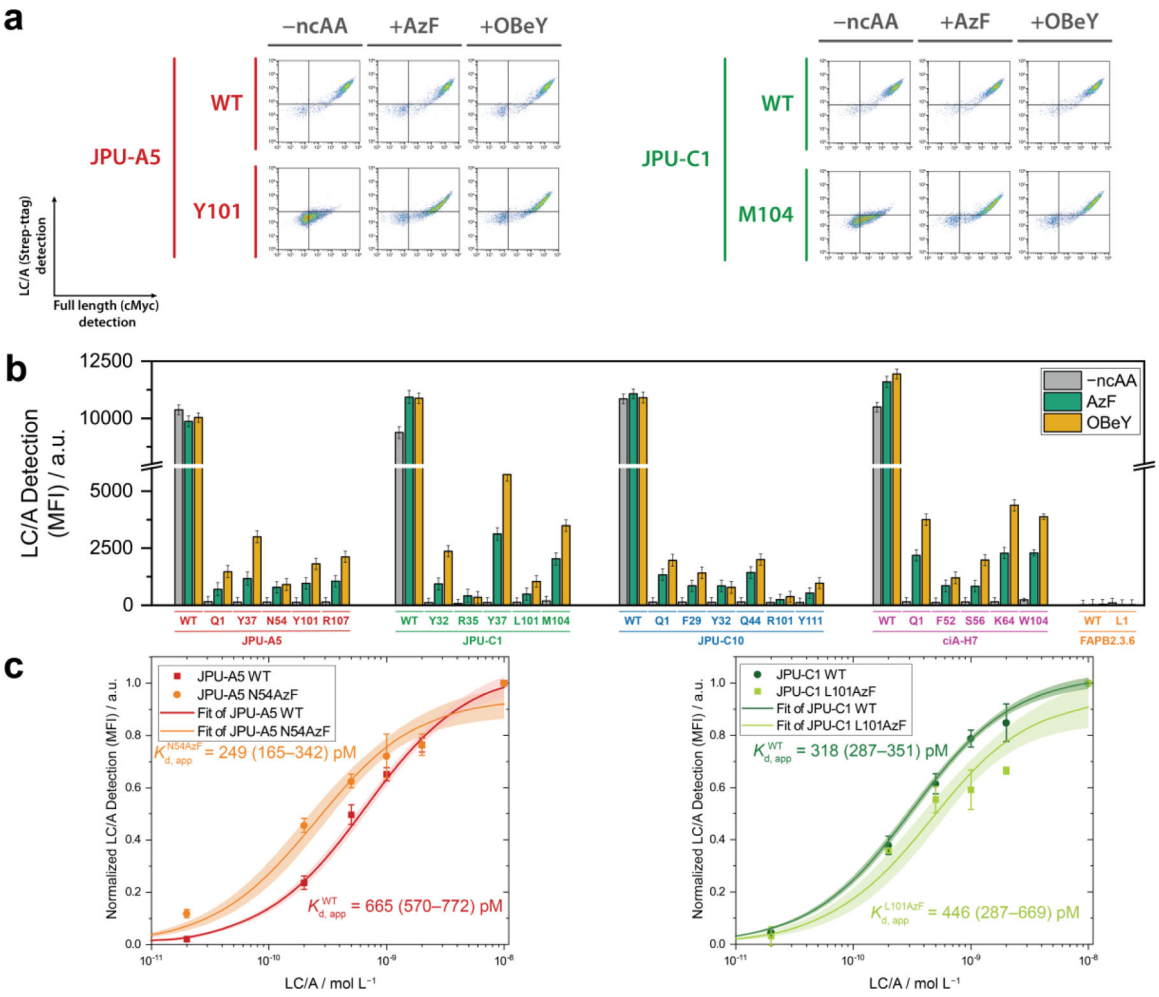

Figure 2.

Binding assays with ncAA-substituted sdAbs. **a** Representative flow cytometry dot plots of displaying yeast cells after induction in the absence of ncAA (−ncAA) or presence of 1 mM AzF or OBeY after incubation with 200 nM LC/A. Cells were labeled against Strep-tag for detection of LC/A (vertical axis) and cMyc tag for full-length displayed antibody (horizontal axis). See Figures S2, S3 for all dot plots. **b** Median fluorescence intensity (MFI) of the LC/A detection of full-length sdAb populations as determined by flow cytometry analysis. The ncAA position is indicated in each case. This experiment was performed once. Error bars represent the robust coefficient of variation of the populations. See Figure S4 for full-length detection MFI. **c** Titration data for selected JPU-A5 (left) and JPU-C1 (right) proteins displayed on the yeast surface. One-site binding fit curves are shown as solid lines and their 95% confidence intervals drawn as shadowed areas. The estimated $K_{d,\,app}$ values are indicated in each plot along with the 95% confidence intervals for each value. The titrations were carried out in technical triplicates. Error bars represent the standard deviation at each concentration. See Figure S5 for titration dot plots.

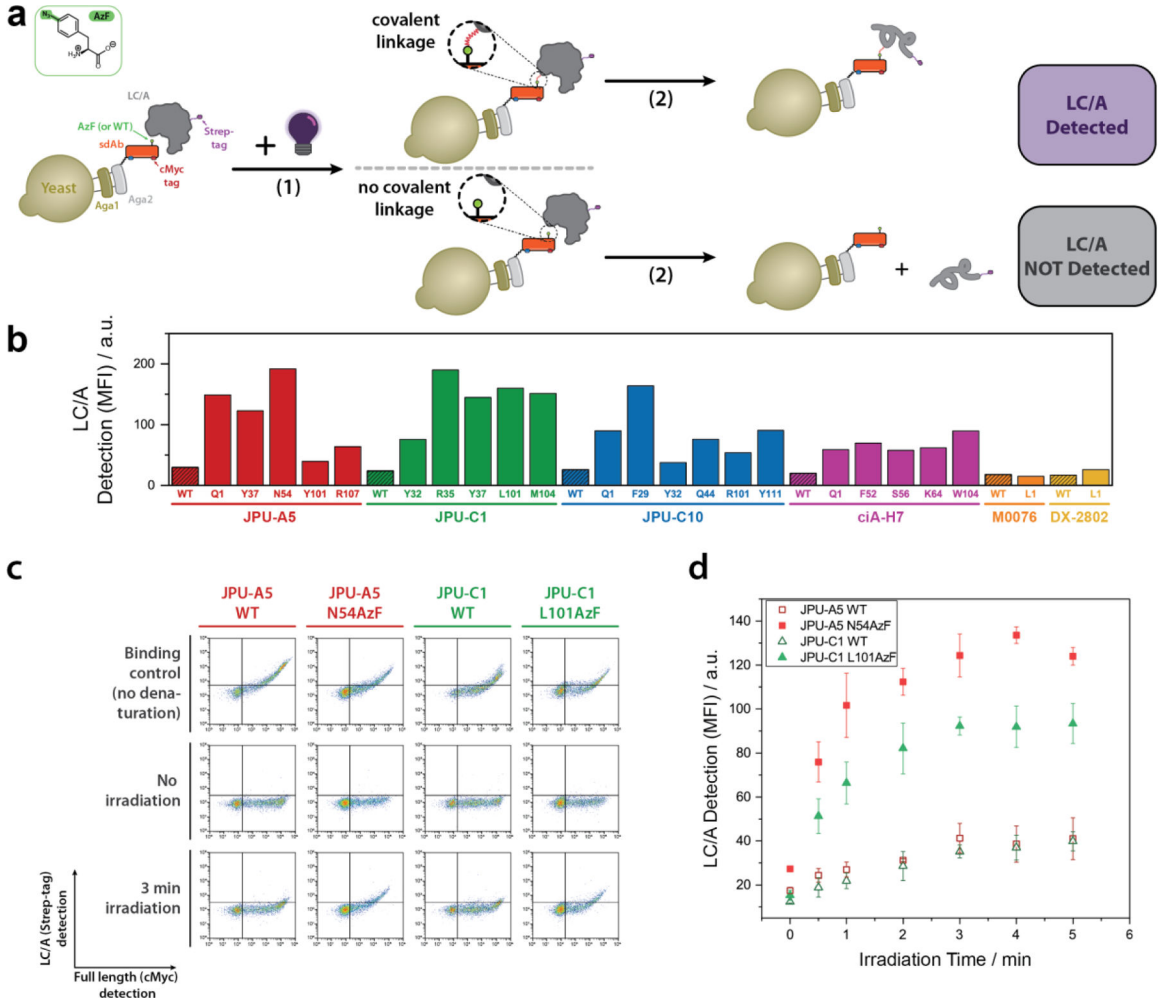

Figure 3.

Identification of photocrosslinkable sdAbs on the yeast surface. **a** Scheme depicting experiments used to characterize photocrosslinking on the yeast surface. Yeast cells displaying sdAbs were incubated with LC/A and subjected to 365 nm UV irradiation (1) which can result in successful crosslinking for some AzF clones (top), but no covalent bond is formed without irradiation, WT, or when AzF mutants cannot covalently bind to the target (bottom). Denaturation (2) removes noncovalently bound LC/A, leaving covalent adducts on the cell surface for detection via flow cytometry. **b** Median fluorescence intensity of LC/A detection in full-length sdAb populations measured via flow cytometry experiments after irradiation for 2 min at 4 °C in a photoreactor and denaturation of yeast displaying the indicated sdAbs, where the residue numbers represent the position where AzF was incorporated. This experiment was performed once. See Figure S7 for all flow cytometry dot plots. **c** Representative flow cytometry dot plots of WT and selected photoreactive sdAbs. The binding control plots show the binding behaviors of displayed sdAbs in the dark, without irradiation or denaturation. The no irradiation and 3 min irradiation panels show the populations of cells after the denaturing step. See Figure S11 for all plots. **d** Time course showing the median fluorescence intensities corresponding to covalent LC/A detection via flow cytometry after the indicated irradiation times for each nanobody. These experiments

were carried out in technical triplicates. The error bars represent the standard deviations of the samples.

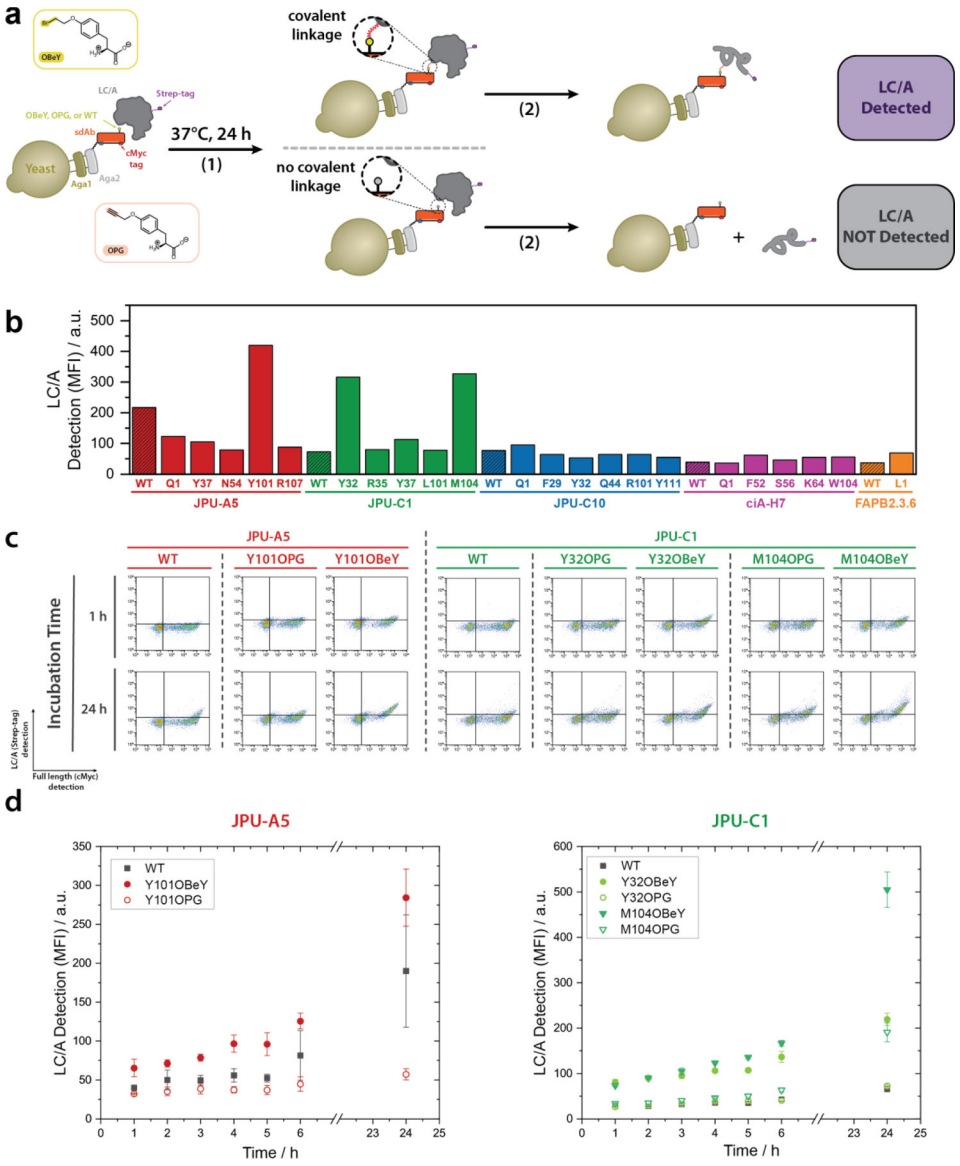

Figure 4.

Identification of spontaneously crosslinkable sdAbs on the yeast surface. **a** Scheme representing the evaluation of spontaneous crosslinking on the yeast surface. Cells displaying sdAbs were incubated with LC/A at 37 °C (1). Certain OBeY-containing clones can form a covalent bond with residues of the nearby LC/A (top), whereas constructs with non-reactive amino acids or that lack the requirements for reactivity maintain a non-covalent interaction (bottom). After denaturation (2), irreversibly bound LC/A can be detected via flow cytometry, while reversible interactions are disrupted, and no LC/A is detected. **b** Median fluorescence intensity of LC/A detection in full-length sdAb populations measured via flow cytometry experiments after incubation with LC/A at 37 °C for 24 h followed by denaturation. Indicated residues correspond to the position where OBeY was incorporated. See Figure S13 for all flow cytometry dot plots. **c** Representative flow cytometry dot plots of WT and OBeY mutants capable of spontaneous crosslinking to LC/A. The corresponding

OPG controls are also included. The flow cytometry analysis was carried out after the denaturation step following different incubation times with LC/A. See Figures S14 and S15 for flow cytometry dot plots. **d** Time course experiment showing the median fluorescence intensities corresponding to LC/A detection via flow cytometry after different incubation times followed by denaturation. These experiments were performed in technical triplicates. The error bars represent the standard deviations of the samples.

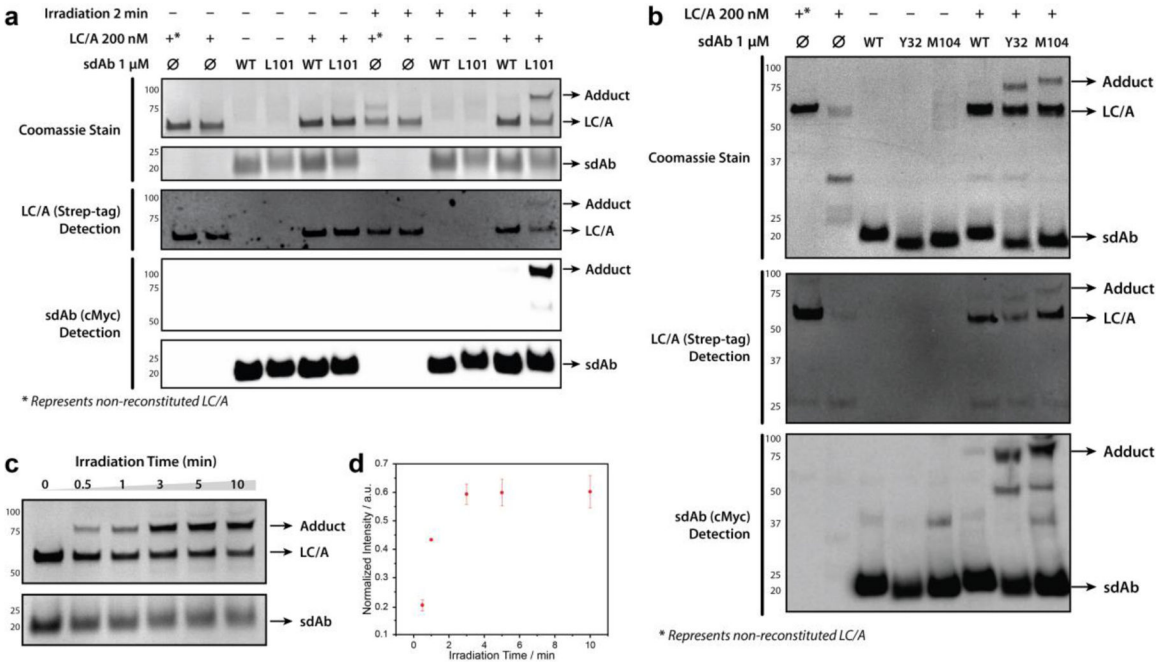

Figure 5.

Crosslinking characterizations of ncAA-sdAbs in solution. **a** SDS-PAGE and western blots of JPU-C1 WT and L101AzF after incubation with LC/A and following 365 nm UV irradiation for 0 or 2 min in solution. A band corresponding to the crosslinked adduct is detected only after irradiation of the L101AzF protein. The western blot results are consistent with the formation of an LC/A-sdAb adduct (Figure S17). **b** SDS-PAGE and western blots of soluble forms of JPU-C1 WT, Y32OBeY, and M104OBeY after incubation with LC/A at 37 °C. The adduct band is observed only in lanes containing OBeY-containing sdAbs, and the western blots further corroborate the identities of the adducts (Figure S18). **c** Time course of the reaction between 1 μM JPU-C1 L101AzF and 200 nM LC/A at different irradiation times as visualized by Coomassie-stained SDS-PAGE (Figure S19). **d** Band intensity of the adduct in the experiment in **c** normalized to that of the LC/A control without incubation or irradiation. This experiment was carried out in technical triplicate. Error bars represent the standard deviations of the samples. LC/A lanes marked with +* indicate inactive LC/A, i.e. in the absence of Zn^{2+}. Western blotting was carried out by probing with Strep-Tactin DY488 1:500 for LC/A detection and mouse α-cMyc HRP conjugate 1:2,500 for sdAb detection.

a

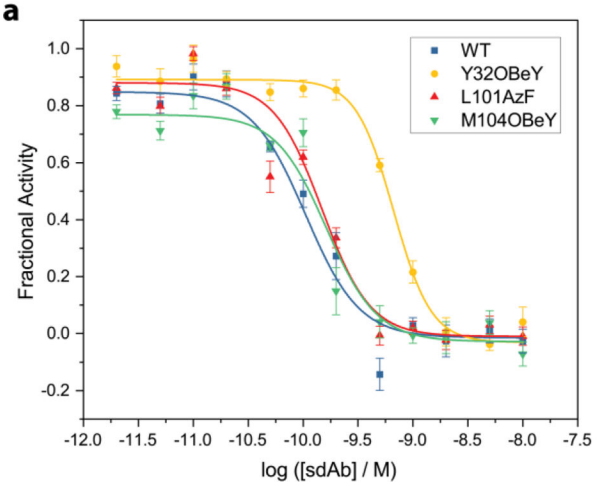

b

sdAb	IC_{50} (95% CI) / pM
WT	106 (78–162)
Y32OBeY	667 (594–765)*
L101AzF	149 (104–219)
M104OBeY	163 (100–313)

* $p < 0.05$

Figure 6.

Evaluation of inhibitory properties of soluble JPU-C1 ncAA-sdAbs. **a** Dose-response curves and **b** estimated IC_{50} values for each sdAb when incubated with 250 pM LC/A followed by addition of 100 nM of fluorescent reporter. Fractional activities were calculated by normalizing the initial rate to that of uninhibited enzyme and fitted to a dose-response model. 95% confidence intervals are shown in parentheses. The starred (*) p-value indicates statistical significance at the 95% level when comparing the IC_{50} value to that of WT. See Figure S21 for kinetic traces.

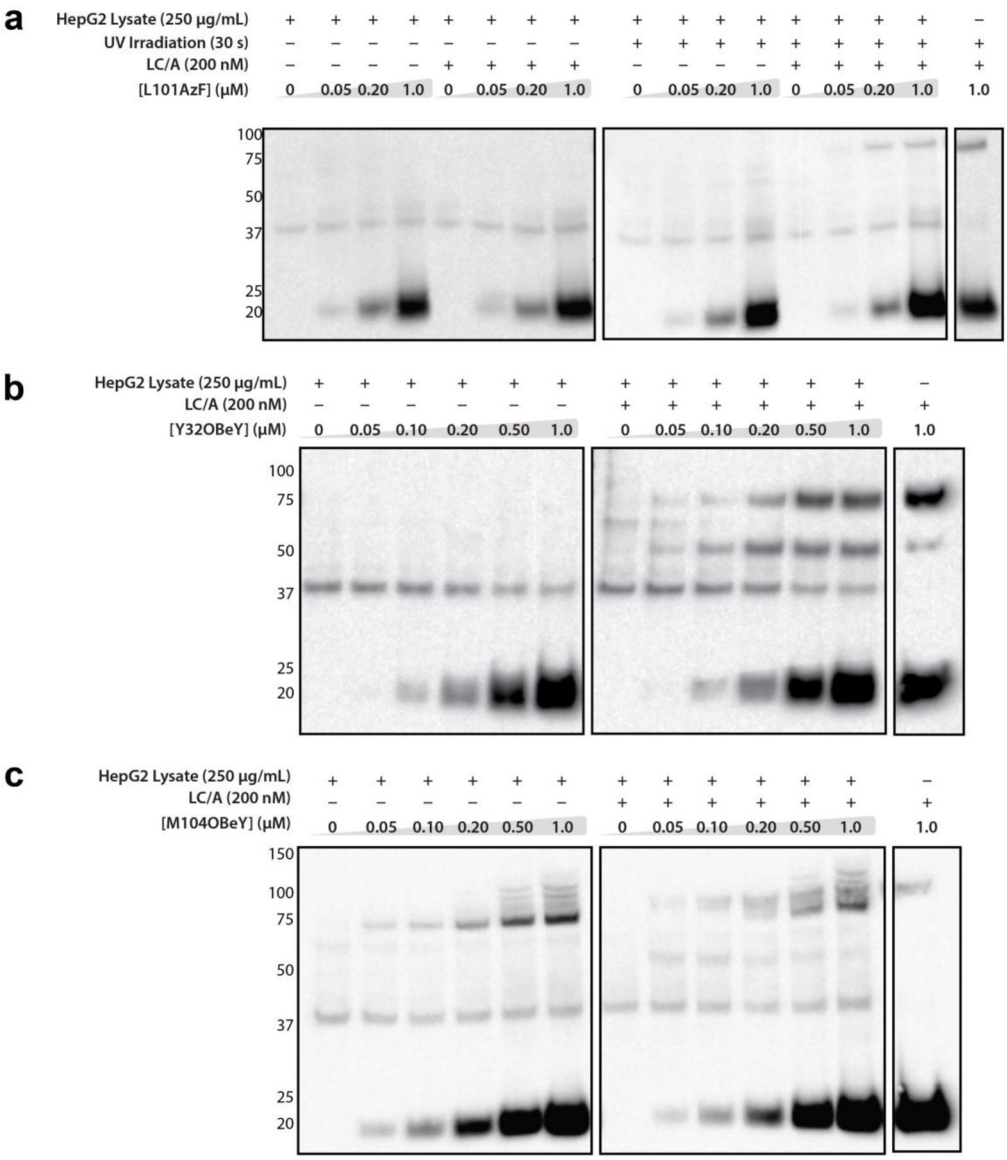

Figure 7.

Evaluation of ncAA-sdAb specificity in the presence of cell lysates. Western blots probed for the sdAb C-terminal cMyc tag after incubation in HepG2 lysate with varying concentrations of **a** JPU-C1 L101AzF, **b** JPU-C1 Y32OBeY, or **c** JPU-C1 M104OBeY, in the presence or absence of 200 nM LC/A. The samples in **a** were analyzed after 1 h incubation at room temperature and with or without 365 nm light irradiation for 30 s. Samples in panels **b** and **c** were incubated for 24 h at 37 °C. The membranes were probed with mouse α-cMyc-HRP conjugate to locate free sdAbs and sdAb adducts. See Figures S22–S24 for Coomassie-stained gels, full cMyc-HRP blots, and Strep-Tactin-DY488 blots. See Figure S25 for intensity profiles of cMyc blots.